Seismic Interpretation of Migrated Data Using Edge-based Geodesic Active Contours

M. Amir Shafiq*, Zhen Wang and Ghassan AlRegib
School of Electrical and Computer Engineering
Georgia Institute of Technology, Atlanta, Georgia 30332–0250
{amirshafiq*, zwang313, alregib}@gatech.edu

***Abstract*—Over the last few years, industry and academia have been shifting towards computer aided models for seismic interpretation because manual labeling and salt dome delineation is becoming very time consuming and labor intensive as the volume of seismic data is in the order of tera-bytes. In this paper, we have proposed an edge-based active contour with an arc length penalty using level set implementation for interpreter-assisted salt dome segmentation. We have designed an edge function and studied the effect of varying different active contour parameters on salt dome boundary detection. Experimental results show the effectiveness of proposed method on the real seismic dataset of F3 block in the North Sea. We have also compared our results with other state of the art methods of salt dome detection and the ground truth which show that active contours are very good candidate for segmenting salt dome.**

***Index Terms*—Seismic Interpretation, Salt Dome Segmentation, Salt Dome Boundary Detection, Active Contours, Level Set Implementation**

I. Introduction

The deposition of salt may penetrate into surrounding rock strata such as limestone and shale to form an important diapir structure, salt domes. Because salt is impermeable, salt domes are effective structural traps that commonly seal petroleum and natural gas. Therefore, accurately locating salt domes is crucial for the exploration of petroleum reservoirs. Experienced interpreters can label the boundaries of salt domes by observing and analyzing seismic signals. With the dramatically growing size of acquired seismic data, however, manually labelling the boundaries is becoming time consuming and labor intensive. To improve interpretation efficiency, in recent years, both industry and academia have used computers to assist the interpretation process. Under the supervision of interpreters, computer-assisted interpretation has been proved to be feasible.

The different formation processes of the salt domes and the surrounding rock strata determine their distinctive appearances in migrated seismic data. By comparing the texture difference between salt and non-salt regions, interpreters can delineate the boundaries of salt domes. To stimulate the visual perception of interpreters, in the last few decades, researchers have proposed computer-assisted salt dome detection methods based on graph theory and image processing techniques. Lomask et al. [1] represented seismic sections as weighted undirected graphs by connecting the edges of two arbitrary vertices with weights, which were determined by the intensity and different positions of the pixels. As an extension of [1], Lomask et al. [2] later employed local dips in the weight matrix and utilized bound constraints to remove boundary artifacts.

Jianbo et al. in [3] proposed that by using normalized cut image segmentation (NCIS), seismic sections can be divided into two parts along salt dome boundaries. Halpert et al. [4] later proposed modified form of NCIS by combining two seismic attributes, instantaneous amplitude and dip variability, with adaptive weights. Although the NCIS-based detection methods can be implemented in parallel, their high computational complexity limits their future application in high-resolution and three-dimensional (3D) seismic data. To speed up the efficiency of image segmentation, on the basis of the minimum spanning tree [5], Halpert et al. [6] applied the pairwise region comparison to the detection of salt domes, which reduces the algorithm complexity from $\mathcal{O}\left(n^2\right)$ to $\mathcal{O}\left(n \log n\right)$.

In addition to segmentation-based methods, edge detection methods are also capable of delineating salt dome boundaries. Both Zhou et al. [7] and Aqrawi et al. [8], convolved dip-guided 2D and 3D Sobel filters, respectively, with time sections and detected the boundaries of salt domes from the obtained gradient maps. Recently, on the basis of supervised Bayesian classification model, Berthelot et al. [9] have proposed extracting the salt dome boundaries from a combination of the three types of seismic attributes: gray-level co-occurrence matrix (GLCM) attributes, frequency-based attributes, and dip and similarity attributes. In addition, Wang et al. [10] and Shafiq et al. [11] have proposed new methods for salt dome detection by introducing novel seismic attributes, 2D and 3D Gradient of Textures (GoT), respectively. Both methods highlight the boundaries of salt domes by evaluating the texture contrast between the two sides of the salt domes.

Over the last few years, researchers have also studied the level set [12] and the active contour models [13], [14], [15], [16] for salt dome segmentation. Automated salt dome extraction from seismic data based on the level set method with a local stop criterion is proposed in [17]. Winston et al. [18] have proposed using level sets to parameterize the salt dome by directly inverting the geometry of salt bodies using full waveform inversion. In this paper, we have proposed to use an edge-based geodesic active contour with an arc length penalty for salt dome detection. The arc length penalty on an edge-based active contour not only forces the dynamic

moving curve to maintain minimum length but also ensures curve smoothness along the salt dome boundary.

The rest of paper is organized as follows. The problem statement is given in section II. Active contours for salt dome segmentation, partial differential equation (PDE) formulation, edge function design and implementation details are introduced in section III. Experimental results are discussed in section IV and finally conclusions are given in section V.

II. Problem Statement

Detecting salt domes from a seismic image falls under segmentation problem and active contours are dynamic curves that move such that the defined energy function is minimized at the object boundaries. If we can formulate an energy function such that it has low values near the salt dome boundary and high values as we move away, then the active contours can accurately segment the salt dome. Our objective is to detect the salt dome boundaries using active contour; however, at the same time, we would like to impose a penalty on curve length to keep it minimum and smooth. In order to achieve this goal, we explicitly define an external and internal energy such that the former will converge the level set curve towards salt dome boundary and the latter will keep the curve smooth. The external energy will be based on the edge detection function whereas the internal energy will be governed by the curve length and the smoothness penalty (parameter λ). We define a parameterized curve $C(p)$, $C_0 : [0, 1] \rightarrow \Re^2$ of Euclidean arc length L and extend it into a time dependent curve $C(p, t)$ such that $C(p, 0) = C_0(p)$. Our energy function is the combination of external and internal energy which is given by (1).

$$E(C(p,t)) = \int_0^L \Phi dp + \int_0^L \frac{1}{2}\lambda \|C_p\|^2 dp \tag{1}$$

In order to minimize energy, we will design a function $\Phi(x, y)$ that will drive the active contours towards the salt dome boundary and penalize the curve length using λ to obtain desired results.

III. Active Contours for Salt Dome Segmentation

In this section, we will formulate our problem into PDE, design function $\Phi(x, y)$ and give details about the level set implementation of the active contours.

A. PDE Formulation

The energy function given by (1) can be minimized using the gradient descent algorithm which will yield a solution given by (2)

$$C_t = -\nabla_c \Phi + \lambda C_{pp}, \tag{2}$$

where C_{pp} is a second order partial derivative of curve $C(p, t)$ with respect to parameter p. Clearly, (2) is not parametrization independent for $\lambda > 0$ and hence is not geometric. We can restate our problem and do the derivation based on the arc length parameter s.

$$E = \int_0^L (\Phi + \frac{\lambda}{2}) ds \tag{3}$$

Let us assume $\Phi(x, y) > 0$ and C is a closed curve or endpoints of a curve. The Euclidean arc length is given by L whereas the weighted arc length is represented by L_ϕ. The calculation of L_ϕ gradient is fairly simple and straight forward.

$$\begin{aligned}\frac{d}{dt}E(C(t)) &= \frac{d}{dt}L_\phi = \frac{d}{dt}\int_0^L (\Phi + \frac{1}{2}\lambda) ds \\ &= \int_0^1 (\Phi_t \|C_p\| + (\Phi + \frac{\lambda}{2})\|C_p\|_t) dp \\ &= \int_0^1 ((\nabla\Phi.C_t)\|C_p\| + (\Phi + \frac{\lambda}{2})C_{tp}.T)) dp,\end{aligned}$$

where $T = \frac{C_p}{\|C_p\|}$. Integrating second term by parts yields

$$\begin{aligned}\frac{d}{dt}E &= \int_0^1 ((\nabla\Phi.C_t)\|C_p\| - C_t[\Phi_p T + (\Phi + \frac{\lambda}{2}).T_p]) dp \\ &= \int_0^1 C_t.(\nabla\Phi - (\frac{\nabla\Phi.C_p}{\|C_p\|})T - (\Phi + \frac{\lambda}{2}).\frac{T_p}{\|C_p\|}) ds \\ &= \int_0^1 C_t.(\nabla\Phi - (\nabla\Phi.C_s)T - (\Phi + \frac{\lambda}{2})T_s) ds,\end{aligned}$$

where $T = C_s = \frac{C_p}{\|C_p\|}$, $T_s = \kappa N = \frac{T_p}{\|T_p\|}$ and $\nabla_c E = \frac{d}{dt}E$

$$\nabla_c E = \int_0^1 C_t.((\nabla\Phi.N)N - (\Phi + \frac{\lambda}{2})\kappa N) ds$$

The energy minimized using gradient descent is given by

$$\begin{aligned}C_t &= -\nabla_c E \\ &= -((\nabla\Phi.N)N - (\Phi + \frac{\lambda}{2})\kappa N) \\ &= \beta N,\end{aligned} \tag{4}$$

where $\beta = (\Phi + \frac{\lambda}{2})\kappa - (\nabla\Phi.N)$ and $\kappa N = C_{ss}$. Equation (4) is the gradient descent update equation for our salt dome segmentation problem.

B. Edge Detection Function

Now, we design the function $\phi(x, y)$ that will dynamically move the active contour towards the salt dome boundary. $\phi(x, y)$ should be chosen such that the energy is minimum when active contour lie accurately on the salt dome boundary. A modified form of the general edge detector for our salt dome detection problem is given by (5)

$$\Phi(x, y) = \frac{1}{(\epsilon + \|\nabla I\| * G_\sigma)^p}, \tag{5}$$

where I is input seismic image, p is positive integer and ϵ is small positive real number in the neighborhood of zero. We have used epsilon in $\phi(x, y)$ function to avoid division by zero that would result in infinite energy if the gradient of image is zero. G_σ is the Gaussian kernel with standard deviation σ and $\|\nabla I\| * G_\sigma$ produces a smooth and denoised version of I so that the active contour don't get stuck in local minima. We have also normalized the image and its edge function to obtain same results for the different seismic images of varying intensities. Function $\phi(x, y)$ is positive in the homogeneous regions of I whereas approximately zero at the salt dome boundary. Typical

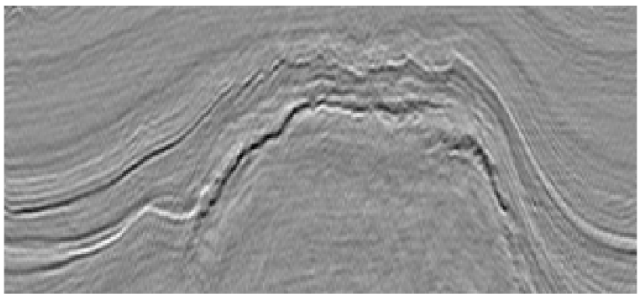

(a)

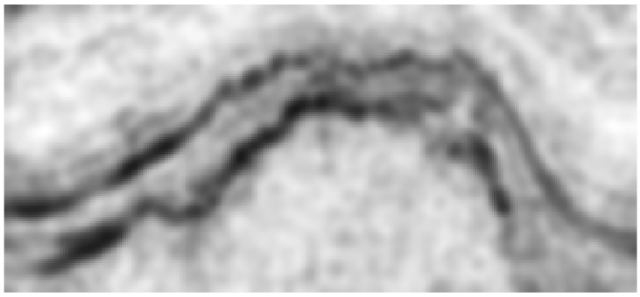

(b)

Fig. 1: (a) Seismic image with salt dome, (b) Edge function $\phi(x, y)$

seismic image containing the salt dome and its edge function $\phi(x, y)$ are shown in Fig. 1. The active contour will move dynamically towards the low values of $\phi(x, y)$ and the energy will be minimized when active contour aligns perfectly with the salt dome boundary.

C. Implementation

The implicit level set evolution [19] of the curve given by (4) can be computed as follows

$$\begin{aligned} \Psi_t &= -\beta\|\nabla\Psi\| \\ \Psi_t &= [(\widehat{\nabla\Phi}.N) - (\widehat{\Phi} + \frac{\lambda}{2})\kappa]\|\nabla\Psi\| \end{aligned} \tag{6}$$

We know that $\kappa = -\nabla.(\frac{\nabla\Psi}{\|\nabla\Psi\|})$, $\|\nabla\Psi\| = \sqrt{\Psi_x^2 + \Psi_y^2}$ and $N = \frac{\nabla\Psi}{\|\nabla\Psi\|}$. Plug these values in (6) to obtain the level set evolution equation as follows

$$\Psi_t = \widehat{\nabla\Phi}.\nabla\Psi + (\widehat{\Phi} + \frac{\lambda}{2})\nabla.(\frac{\nabla\Psi}{\|\nabla\Psi\|})\|\nabla\Psi\| \tag{7}$$

We have used the upwind forward time difference scheme for numerical implementation of (7)

$$\begin{aligned} \Psi(t + \Delta t) &= \Psi(t) + \Delta t(\widehat{\nabla\Phi}.\nabla\Psi + \\ &\quad (\widehat{\Phi} + \frac{\lambda}{2})\nabla.(\frac{\nabla\Psi}{\|\nabla\Psi\|})\|\nabla\Psi\|) \end{aligned} \tag{8}$$

The term $\nabla.(\frac{\nabla\Psi}{\|\nabla\Psi\|})\|\nabla\Psi\|$ is the geometric heat equation and can be implemented numerically using (9).

$$\nabla.(\frac{\nabla\Psi}{\|\nabla\Psi\|})\|\nabla\Psi\| = \frac{\Psi_x^2\Psi_{yy} - 2\Psi_x\Psi_y\Psi_{xy} + \Psi_y^2\Psi_{xx}}{\Psi_x^2 + \Psi_y^2}$$

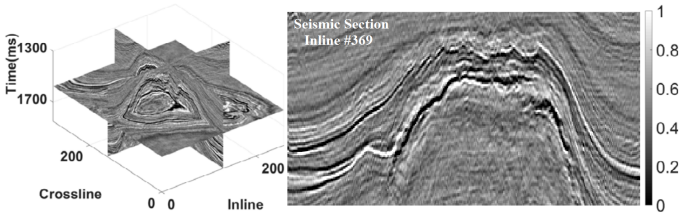

Fig. 2: Tested volume and seismic section inline #369

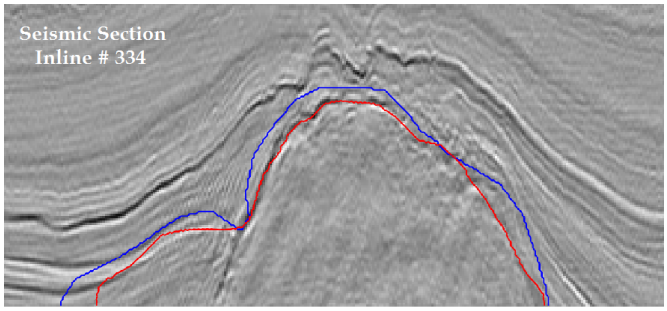

(a)

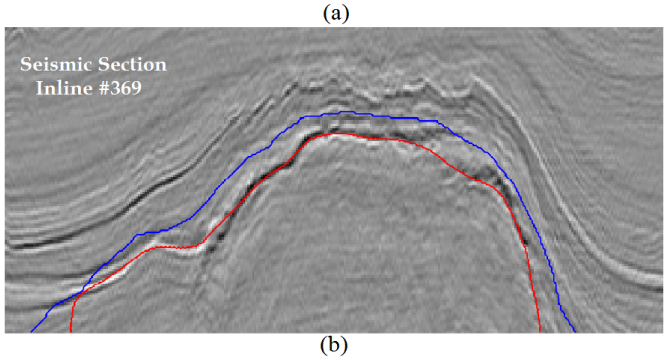

(b)

Fig. 3: Initial and final level set curve

$\nabla\Psi = [\Psi_x; \Psi_y]$ and the heat equation were computed using the central difference. $\widehat{\Phi}$ and $\widehat{\nabla\Phi}$ are extensions of Φ and $\nabla\Phi$, respectively, computed after every thirty iterations.

IV. Experimental Results

In this section, we will present the results of active contour and other methods for salt dome segmentation. We have used the real seismic dataset acquired from the Netherland offshore $F3$ block in the North Sea, whose size is 24 x 16 km^2. The seismic volume that contains the salt dome structure has an inline number ranging from $\#151$ to $\#500$, a crossline number ranging from $\#401$ to $\#701$, and a time direction ranging from $1,300ms$ to $1,848ms$ sampled every $4ms$. Fig. 2 illustrates the tested seismic volume and one of its seismic sections, inline $\#369$.

Fully automated salt dome detection occasionally fails to perform adequately because it may pick up seismic areas that are of no or little interest to geophysics interpreters. Therefore, interpreter-assisted salt dome detection is not only robust but is also infallible to false positives. The edge-based active contour may get stuck in the local minima and do not get to the desired salt dome boundary if the zero level set is initialized very

TABLE I: Frechet Similarity

Methods	Inline #334	Inline #369
Aqrawi et al. [8]	0.7048	0.9351
Bretholt et al [9]	0.8463	0.9194
Shafiq et al. [11]	0.8595	0.9378
Proposed	0.9470	0.9640

far from the ground truth in seismic sections which contain multiple dips near the salt dome boundary. To overcome this drawback and make the level set convergence robust to local minima and fast, we initialized the zero level set curve near the salt dome boundary. We have used the initial level set estimate as input by an expert geophysicist in the vicinity of the salt dome and the active contour will fine tune itself and detect the salt dome boundary. The initial level set (blue) and the final level set curve (red) after evolution in inline #334 and #369 are shown in Fig. 3(a)–(b), respectively, which illustrates that the active contour successfully segmented salt dome.

We also compared our results with the detection methods presented in [8], [9] and [11]. Fig. 4(a)–(b) compares salt dome boundaries detected by different methods in inline #334 and #369, respectively, with the ground truth manually labeled in green. The magenta, yellow and blue lines represent the boundaries detected by [8], [9] and [11] whereas the red line represents the boundary detected by the proposed method. Subjectively, it can be observed that active contour performs the best among all other methods of salt dome segmentation. To objectively evaluate the similarity between the detected boundaries and the ground truth, we normalized the Frechet distance [10], [20] into a similarity index. A similarity index close to one indicates that the detected salt dome boundary and the ground truth are close to each other whereas indices close to zero show a dissimilarity between the two curves. Frechet similarity indices of the detected salt dome boundaries in inlines #334 and #369 are shown in Table I. Among all methods, the active contour performs best with a similarity of 94.7% and 96.4% in inlines #334 and #369, respectively.

In order to study the effects of the active contour parameters on the salt dome segmentation, we ran experiments with different values of λ and plotted similarity indices in Fig. 5. The effectiveness of the active contour can be seen from the fact that even choosing different values of λ provides better results as compared to those achieved by the other methods of salt dome boundary detection.

V. Conclusion

Although fully automatic salt dome detection may occasionally fails to perform successful segmentation, interpreter guided semi-automated segmentation makes seismic interpretation more robust and accurate. In this paper, we presented an edge-based active contour with an arc length penalty to detect the boundaries of the salt domes in seismic images. Our experimental results show that the presented method outperforms state of the art methods for salt dome detection. The results presented in this paper demonstrate that the active contour

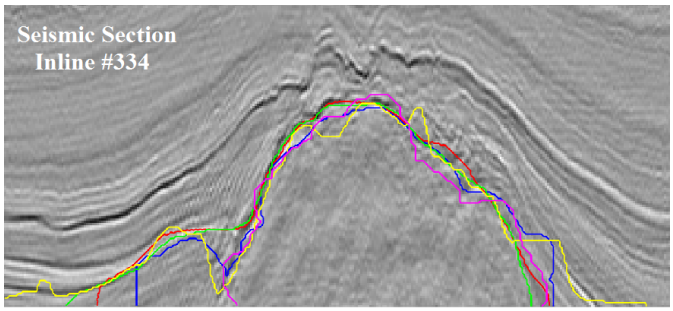

(a)

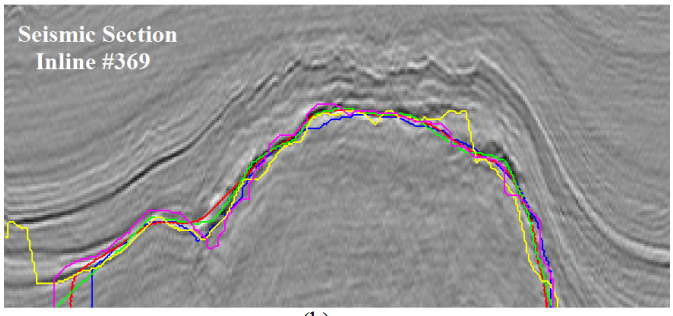

(b)

Fig. 4: Comparison of boundaries detected by different methods with ground truth

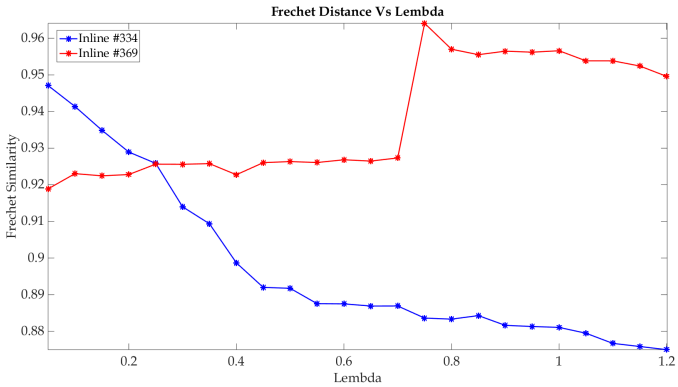

Fig. 5: Frechet similarity vs lambda

are very good candidate for semi-automated interactive salt dome segmentation. We also presented the effect of parameter variations on salt dome segmentation, which demonstrates that even without fine tuning of parameters, the active contour performs better as compared to the other salt dome detection methods, which qualifies the active contour as a very good method for salt dome detection. Furthermore, since we are using a zero level set as input from an expert geophysicist, the current work can be extended to the tracking of salt dome boundaries across seismic volume and hence eliminate the need of initialization at each seismic inline.

Acknowledgment

This work is supported by the Center for Energy and Geo Processing (CeGP) at Georgia Tech and King Fahd University of Petroleum and Minerals (KFUPM).

REFERENCES

[1] Jesse Lomask, Biondo Biondi, and Jeff Shragge, "Image segmentation for tracking salt boundaries," in *Expanded Abstracts of the SEG 74th Annual Meeting*, 2004, pp. 2443–2446.

[2] Jesse Lomask, Robert G. Clapp, and Biondo Biondi, "Application of image segmentation to tracking 3D salt boundaries," *Geophysics*, vol. 72, no. 4, pp. P47–P56, 2007.

[3] Jianbo Shi and Jitendra Malik, "Normalized cuts and image segmentation," *Pattern Analysis and Machine Intelligence, IEEE Transactions on*, vol. 22, no. 8, pp. 888–905, 2000.

[4] Adam D. Halpert, Robert G. Clapp, and Biondo Biondi, "Seismic image segmentation with multiple attributes," in *Expanded Abstracts of the SEG 79th Annual Meeting*. Society of Exploration Geophysicists, 2009, pp. 3700–3704.

[5] Pedro F. Felzenszwalb and Daniel P. Huttenlocher, "Efficient graph-based image segmentation," *International Journal of Computer Vision*, vol. 59, no. 2, pp. 167–181, 2004.

[6] Adam D. Halpert, Robert G. Clapp, and Biondo Biondi, "Speeding up seismic image segmentation," in *Expanded Abstracts of the SEG 80th Annual Meeting*. Society of Exploration Geophysicists, 2010, pp. 1276–1280.

[7] Jing Zhou, Yanqing Zhang, Zhigang Chen, and Jianhua Li, "Detecting boundary of salt dome in seismic data with edge detection technique," in *Expanded Abstracts of the SEG 80th Annual Meeting*. Society of Exploration Geophysicists, 2007, pp. 1392–1396.

[8] Ahmed Adnan Aqrawi, Trond Hellem Boe, and Sergio Barros, "Detecting salt domes using a dip guided 3D Sobel seismic attribute," in *Expanded Abstracts of the SEG 81st Annual Meeting*. Society of Exploration Geophysicists, 2011, pp. 1014–1018.

[9] Angélique Berthelot, Anne HS Solberg, and Leiv J. Gelius, "Texture attributes for detection of salt," *Journal of Applied Geophysics*, vol. 88, pp. 52–69, 2013.

[10] Zhen Wang, Tamir Hegazy, Zhiling Long, and Ghassan AlRegib, "Noise-robust detection and tracking of salt domes in post-migrated volumes using texture, tensors, and subspace learning," in *submitted to Geophysics*, 2015.

[11] Muhammad A. Shafiq, Zhen Wang, Asjad Amin, Tamir Hegazy, Mohamed Deriche, and Ghassan AlRegib, "Detection of salt-dome boundary surfaces in migrated seismic volumes using gradient of textures," in *2015 SEG 85th Annual Meeting, New Orleans, Louisiana, Oct. 18-23*, 2015.

[12] J. A. Sethian, "Evolution, implementation, and application of level set and fast marching methods for advancing fronts," *Journal of Computational Physics*, vol. 169, pp. 503–555, 2001.

[13] M. Kass, A. Witkin, and D. Terzopoulos, "Snakes - active contour models," *International Journal of Computer Vision*, vol. 1, no. 4, pp. 321–331, 1988.

[14] T. Chan and L. Vese, "Active contours without edges," *IEEE transactions on image processing*, vol. 10, no. 2, pp. 266–277, 2001.

[15] D. Mumford and J. Shah, "Optimal approximation by piecewise smooth functions and associated variational problems," *Comm. Pure Appl. Math*, vol. 42, pp. 577–685, 1989.

[16] Anthony Josephy Yezzi, "Advanced computer vision and image processing using pdes and active contour," *Partial Differential Equations in Image Processing and Computer Vision*, Jan. 2011.

[17] Jarle Haukas, Oda Roaldsdotter Ravndal, Bjorn Harald Fotland, Aicha Bounaim, and Lars Sonneland, "Automated salt body extraction from seismic data using level set method," *First Break, EAGE*, vol. 31, Apr 2013.

[18] Winston Lewis, Bill Starr, and Denes Vigh, "A level set approach to salt geometry inversion in full-waveform inversion," *SEG Las Vegas 2012 Annual Meeting*, 2012.

[19] Gabriel Peyre, "Active contours using level sets," *Numerical Tours*, 2010.

[20] Helmut Alt and Michael Godau, "Computing the Fréchet distance between two polygonal curves," *International Journal of Computational Geometry & Applications*, vol. 5, no. 01n02, pp. 75–91, 1995.